L. Erlbeck, D. Wössner, T. Kunz, M. Rädle and F.-J. Methner

Investigating Freeze Crystallization as Promising Next-generation Water Purification Technology for the Brewing Industry

Water purification is important in the brewing industry, even more so when the possibility of water scarcity in the immediate future is considered. The current water purification technologies have the disadvantage that they require many chemicals and are not easily paired with renewable energies. Freeze crystallization can potentially be an alternative for which no chemicals are necessary. A multi-step process, consisting of a commercial scraped surface crystallizer, in combination with a self-made pressing mold, were used to investigate the possibility of purifying water with this technology. Results show that it is feasible to reduce the residual alkalinity significantly. A pressing force of 7.7 kN (20.6 bar), and a holding time of 300 s, were found to be sufficient. A seawater desalination-based design was then used to investigate water purification using a single-step process, which consisted of a screw conveyor as scratcher, and a perforated, tapering cone for ice pressing. The results showed good removal efficiencies for manganese, total organic carbon, residual alkalinity, and nitrate depending on the rotational speed and coolant temperature. Heat flows, heat transition coefficients, and ice crystal areas underpinned assumptions. Finally, one correlation was found to best reflect experimental and calculated results.

Descriptors: brewing water, freeze crystallization and ice pressing, water purification, water treatment

1 Introduction

Water purification, and therefore water supply, is one of the most significant problems to be solved in the immediate future. *Townsend*, for example, already pointed out that water scarcity can significantly lower the GDP of a country, if not prevented in a timely manner [1]. This is, of course, a prominent interest of the beverage industry, and especially the brewing industry, where water is used in many of their processes: mashing, boiling, fermentation, maturation, separation and rinsing [2, 3]. As an average, 4.2 liters of clean water are used to produce one liter of beer, and this quantity could potentially be higher for small- or medium-sized breweries [4–6]. Therefore, avoiding waste can lower production costs. Small- and medium-sized breweries are of main interest in this respect because of their out-of-date facilities, combined with the possibility of their being willing to use different and innovative, yet not fully developed, technologies more readily than large-scale plants [7].

Natural water sources cannot directly be used because of their contamination with different ions and microorganisms. The most common water pollution that disturbs the brewing process, including the beer taste afterwards, is normal calcification, which effects the pH-value during mashing [8]. Iron and manganese concentrations influence yeast, thus disrupting the fermentation process, taste, and flavor stability [9, 10]. Overfertilization in natural water sources causes acceleration of nitrate concentrations, negatively influencing the yeast as well [11]. Furthermore, the excessive use of pharmaceuticals and pesticides lead to organic residues in water with yet unknown impacts on humans as well as on the brewing process [12].

The most predominantly used water purification technologies in the brewing industry are the reverse osmosis and ion exchanger technologies [13]. Both technologies are well known and widespread but have the disadvantage of requiring a significant use of different chemicals, rendering them unsuitable as environmentally friendly processes [14]. Important factors for realization of new technologies depend heavily on the cleaning process itself and the workability. However, affordability and environmental friendliness are at least as important as technical issues. Accordingly, an alternative and prospective technological solution can be water purification via freeze crystallization [15]. The process includes heat pumps to use the thermal energy derived on conversion from electrical energy. Thus, the advantage of small temperature gradients through heat recovery leads to a high coefficient of performance (COP). As a result, smaller energy production plants are necessary, thereby reducing investment costs [16]. A rough calculation leads thereby to a comparison of a theoretical energy demand of around 10 kWh/m³ for freeze crystallization and less than 1 kWh/m³ for reverse osmosis, respectively. For any standard application reverse osmosis as well as ion exchanger are reasonable in an energetic point of view. However, the aim of the investigation is to develop a tech-

https://doi.org/10.23763/BrSc18-08erlbeck

Authors

Lars Erlbeck, Dirk Wössner, Matthias Rädle, Institute for Process Control and Innovative Energy Conversion, University of Applied Sciences Mannheim, Mannheim, Germany; Thomas Kunz, Frank-Jürgen Methner, Chair of Brewing Science, Department of Food Technology and Food Chemistry, Technical University of Berlin, Berlin, Germany; corresponding author: Lars Erlbeck, l.erlbeck@hs-mannheim.de

nology which can be used to produce process water independent from conventional energy sources. Considering this fact, reverse osmosis is still expensive when powered by renewable energy sources only and is therefore not economically viable for a self-sufficient water supply or independent production of process water [17, 18]. A more detailed calculation for freeze crystallization but for seawater desalination confirmed this assessment [19]. Therefore, with lack of necessary chemicals, the possibility to use renewable energy sources in combination with heat pumps, and the chance of arbitrarily scaling the process freeze crystallization appears to be ideal to generate process water for the beverage industry.

Although known for many years, freeze crystallization never moved beyond basic research besides at a few demonstration plants [20]. The general process of freeze crystallization is based on the physical effect of ion expulsion from growing crystals when ice is formed, by lowering the temperature of the solution to the freezing point, and further thermal energy is extracted. In pure crystals, concentrated brine is trapped within intercrystalline channels or pores. The volumes of those channels increase along with the concentration of ions in the feed water until complete volumes can be seen [21, 22]. Changing operation conditions, such as the temperature or turbulence of the solution, or intensifying the heat contact, causes variation in growth rates. Higher growth rates lead to more complex ramifications in the ice crystal, and to more narrow channels with higher streaming resistance and less ion expulsion [22]. This happens when the solution surrounding the ice has a higher concentration, and thus a lower freezing point, than the rest of the solution. This inhibits further crystal growth at this point of the ice front, but forces growth at another point, which then causes liquid inclusions. This is preventable through higher turbulence of the liquid to reduce the concentration gradient near the ice front [23].

This freezing process is already familiar within the food industry where it is used to concentrate juices [24–26], milk [27], milk protein [28], coffee [29–33], and sugar solutions [34], but not for cleaning water. Frequently-used freezing technologies include block ice, round cell, suspension- and plate-crystallization [21, 35–39]. The main point of these experiments is that it is not possible to obtain potable water without any post-treatment, and the typical process is washing the product with melted clean water, which leads to a loss of product.

Therefore, this study, based on previous investigations on water purification processes and several post-treatments [15], investigated freezing crystallization, in combination with pressing, as a batch-process, consisting of a continuous screw crystallizer and a pressing mold for a 50-ton press to purify water as a source for the brewing industry. Furthermore, based on these results, a new plant was developed that combines freezing and pressing to gain a continuously potable water-producing test plant.

2 Materials and methods

2.1 Reagents

Samples were prepared prior to experiments using tap water from

Nomenclature

Symbols

A	Area [m²]
C	Constant [-]
c	Concentration [mg/l]
d	Diameter [m]
F	Pressing force [N]
Fr	Froude number
g	Gravity [m/s²]
h	Heat transition coefficient [W/(m² K)]
K	Hardness [° dH]
l	Length [m]
m	Mass [kg]
$\dot{m}$	Mass flow rate [kg/s]
n	Rotational speed [1/s]
Nu	Nusselt number [-]
Pr	Prandtl number [-]
q	Volumetric flow rate [m³/s]
R	Removal efficiency [%]
RA	Residual alkalinity [mmol/l]
Re	Reynolds number [-]
t	Time [s]
u	Velocity [m/s]
w	Mass fraction [%]

Greek

α	Heat transfer coefficient [W/(m² K)]
β	Screw pitch [°]
γ	Coefficient [-]
ε	Coefficient [-]
η	Dynamic viscosity [Pa*s]
ϑ	Temperature [°C]
κ	Coefficient [-]
λ	Heat conductivity [W/(m K)]
ρ	Density [kg/m³]
φ	Volume fraction [%]

Subscripts

a	Axial
$B\&A$	Bott & Azoory
$B\&L$	Bel and Lallemand
e	Equivalent
el	Electrical
f	Fluid
fl	Flow
i	Inner
l	Liquid
m	Mixture
o	Outer
r	Rotor shaft
S	Stirred
s	Solid
St	Stein
Sc	Screw/scraper
TWH	Total water hardness
t	Tangential
W	Vessel wall
Z	Zlokarnik

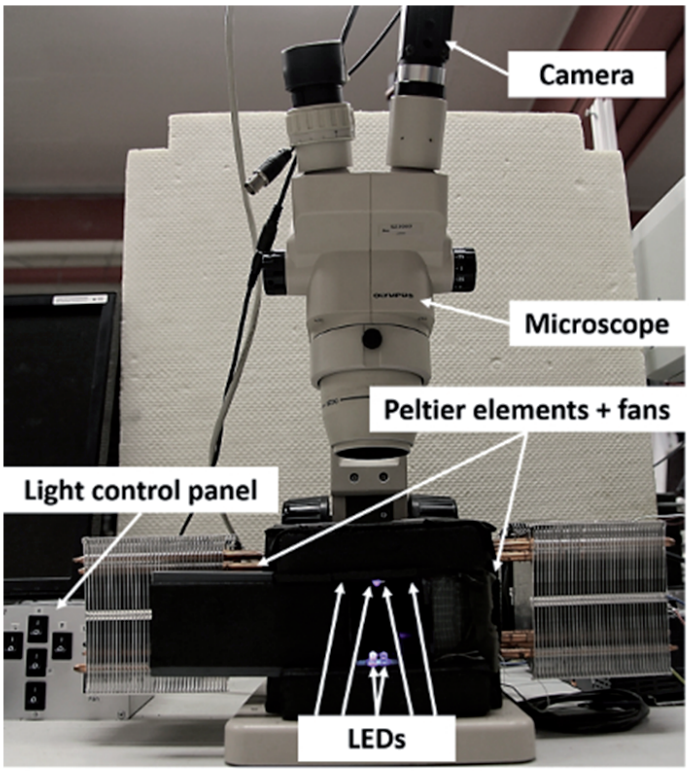

Fig. 1 Microscope with camera and cooling chamber

Mannheim, Germany, which is quite contaminated with carbonates. Further additives, simulating any contaminations like iron chloride, ammonia nitrate, manganese sulfate and urea, were purchased from Sigma-Aldrich. The ions and concentrations of the feed were thereby chosen by really occurring values and substances. These concentrations, as can be seen for the TOC and nitrate concentrations, are realistic for harsh conditions as standing water bodies which can occur in rural or remote areas [40–42]. Additionally, an initial solution volume of 30 l was prepared and utilized until exhausted. The crystallizer was consistently flushed with test solution prior to experiments.

2.2 Sample analysis

To determine the ion concentration in the water, brine, or melted ice, a Dr. Lange CADAS 200 photometer was used. Test kits for calcium, magnesium and total water hardness (LCK327), nitrate (LCK 340), total organic carbon (TOC) (LCK 380), iron (LCK 521) and manganese (LCK 532) were purchased from Hach Lange GmbH. The value for TC was thereby calculated from the photometer measuring the total inorganic carbon as well.

For a better understanding of the dependency between ice particle size and its purity, crystal structure analysis was conducted using a self-made cooling chamber (Fig. 1). In this chamber, the temperature could be adjusted fitting the crystallization temperature, and thus, ensuring a stable ice shape from sample collection until analysis. Consistent lighting was achieved via several light-emitting diodes (LEDs), placed at the inner top and bottom of the chamber, which made it possible to change between incident light and transmitted light. Therefore, the LEDs could be switched on separately. In addition to white LEDs, ultraviolet LEDs were installed as well. Furthermore, double-glazing was utilized in combination with enclosed moisture traps to prevent any condensed vapor while ensuring light for the microscope.

Two Peltier elements from RS Components (Supercool® PC-072-14-06) cooled the chamber, while one computer fan from Thermaltake (Contac 21) each aided with heat dissipation. Heat convection within the chamber was improved by a small fan (SEPA MFB25B12), while cooling reservoirs (cooling ribs) ensured heat storage when the chamber was open to place the sample. A Peltier element controller purchased from uwe electronic (UETR-MOST-16A and Peltier-Cooling Unit 12V) powered the Peltier elements. The microscope itself was a SZ30 from Olympus, combined with an ImagingSource camera (DFK 23G445) with a resolution of 1,280 x 960.

The image analysis software, ImageJ from the National Institutes of Health, USA, was used [43]. Crystals were manually identified and measured because of their complex geometry and low contrast to the surrounding liquid (Fig. 2). The camera provided a resolution of 11.316 pixel/µm. For further evaluation, the median of the crystal area and the standard deviation were calculated.

All samples were taken directly after crystallization, or after leaving the cone, and were then placed into the cooling chamber. Overall, tests were consistently carried out three times.

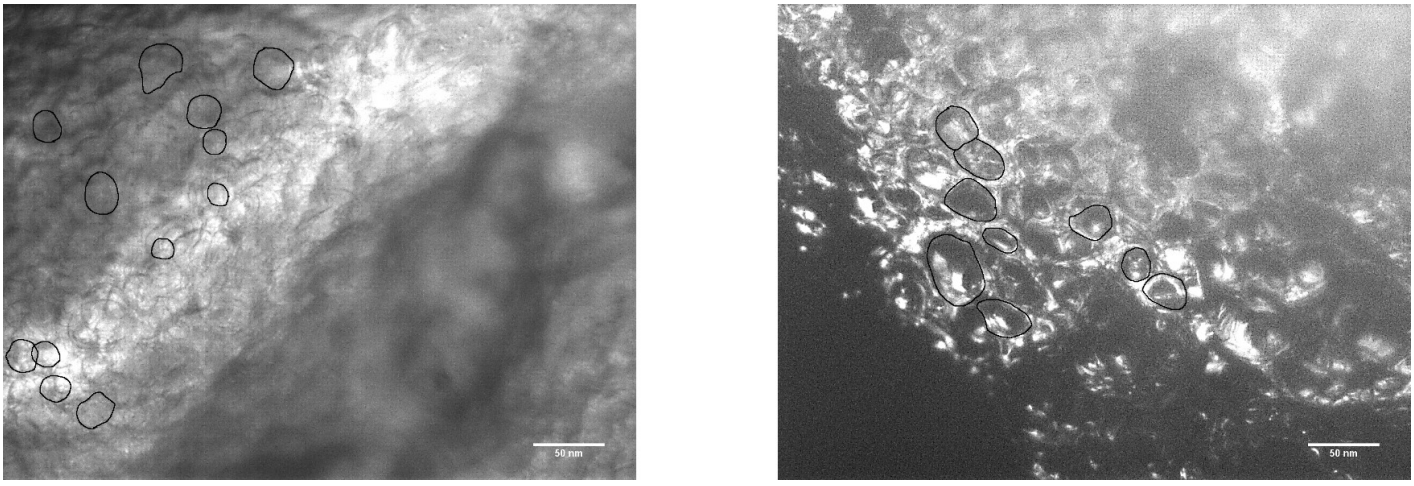

Fig. 2 Exemplary images of non-pressed (left) and pressed ice (right) with traced particles ($l_{Scale} = 50\ nm$)

2.3 Data analysis

Experimental results were used to calculate the removal efficiency (R) using the concentration of the ice (c_{Ice}) and the feed (c_{Feed}) (Eq. 1). For clarity, the removal efficiency is shown as a box plot, which allows an easier understanding of the data and their distribution. Therefore, the box is divided in a 25th and 75th percentile, and the median and the mean values are shown as line and square, respectively. Furthermore, the outliers are shown as 5th and 95th percentile. However, all removal efficiencies for all ions for one test parameter are included in one box.

The residual alkalinity was calculated using equation 2, equation 3, and equation 4 but with the total water hardness instead of carbonate hardness only [44].

$$R = \left(1 - \frac{c_{Ice}}{c_{Feed}}\right) * 100\% \quad \text{(Eq. 1)}$$

$$K_{Ca^+} = \frac{c_{Ca^{2+}}}{7.15} \quad \text{(Eq. 2)}$$

$$K_{Mg^+} = \frac{c_{Mg^{2+}}}{4.34} \quad \text{(Eq. 3)}$$

$$RA = \frac{K_{TWH} - \frac{K_{Ca^{2+}}}{3.5} - \frac{K_{Mg^{2+}}}{7}}{5.6} \quad \text{(Eq. 4)}$$

3 Experimental setup and results

Based on a multi-step plant, the purification of water was analyzed. Subsequently, a single-step plant was built, which is described and evaluated further on in the paper. The setups were investigated to determine whether they can be used to produce process water for the brewing industry, and what the dependencies of pressing force, holding time, coolant temperature, and rotational speed are on ice purity.

3.1 Multi-step plant (semi-batch process)

One easy way to produce ice is to use a scratcher with a fixed heat transfer surface and a double jacket for the coolant. Such Scraped Surface Crystallizers (SSC) already exist for the production of ice slurry for cooling purposes [45].

3.1.1 Experimental setup

An SSC was, therefore, obtained from Wittmann Kältetechnik GmbH & Co. KG. This plant was equipped with a screw as scratcher and forced conveyor, a double jacket in which the coolant vaporized, and an outlet which was positioned orthogonally to the conveying direction at the top of the plant (Fig. 3). A pressing mold, provided with a double jacket for coolant to prevent the sweating effect, in combination with a commercial 50 t press was used for post-treatment. A cooling temperature that was appropriate either to the freezing temperature of the solution or the cooling temperature of the crystallizer was chosen. Outlet of the concentrated solution was achieved via 44 evenly-arranged perforations at the lower part of the pressing mold, where the main pressing takes place. [15]

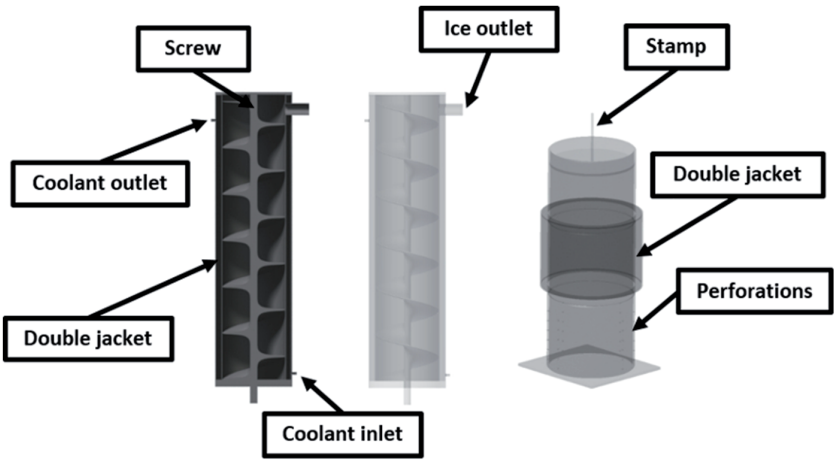

Fig. 3 Schematic sectional drawing of the screw crystallizer and the pressing mold

3.1.2 Results and discussion

Producing ice from usual tap water with such a screw crystallizer, and pressing it with a force of 7.7 kN (20.6 bar), for a holding time of 300 s, results in different ice qualities, as can be seen in figure 4. The separated ice has an ice has an already-lower concentration than the feed. Pressing the ice results in an even lower concentration and standard deviation, which allows for the customization of the ice concentration by adjusting the pressing force and/or holding time.

Overall, results show that it is possible to reduce the hardness of well water by freezing the water to ice and subsequently separating the ice from the concentrated solution by pressing.

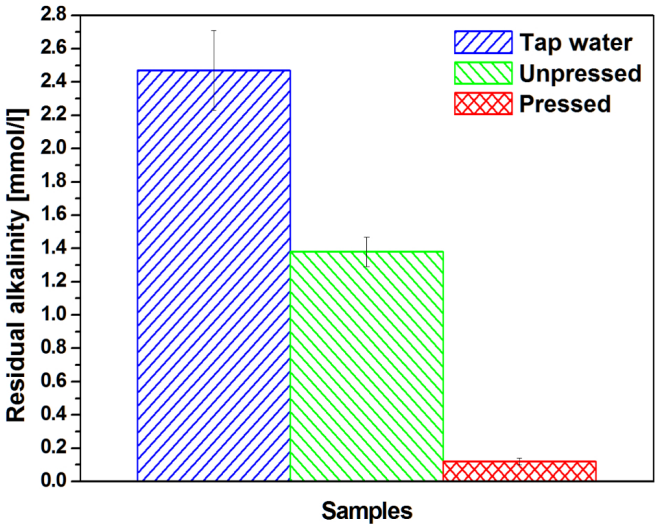

Fig. 4 Purity of tap water, unpressed ice, and pressed ice
$(\vartheta_{Vaporization} = -14.5\ °C, m_{Feed,Press} = 1{,}000\ g,$
$\vartheta_{Press} = 0\ °C, t_{Press} = 300\ s, F_{Press} = 7.7\ kN)$

Table 1 Results of the experiments with tap water using an SSC in combination with a pressing mold

Description	Unit	Parameter
Heat flow	[W]	519.7
Temperature difference	[K]	27.1
Logarithmic temperature difference	[K]	23.4
Screw pitch	[deg]	12
Screw diameter	[m]	0.045
Inner vessel diameter	[m]	0.047
Length cooling area	[m]	0.137
Inner heat transfer area	[m²]	0.020
Heat transition coefficient	[W/(m² K)]	678.5
Rotational speed	[1/min]	10.0
Pressing power press	[kN]	7.7
Holding time press	[s]	300

3.1.3 Key technical data

The whole plant was a commercial product. Thus, no detailed design data are known or can be used for analyses. Nevertheless, different correlations that can be used for the evaluation of the experimental results already exist. For these correlations, a knowledge of various parameters is required. These are listed in table 1.

3.2 Nusselt correlations

It was not possible to determine any heat transfer coefficients separately. Thus, two general and two specific Nusselt correlations were compared for usability. One was suggested by *Stein* [46] (Eq. 5) and is used to characterize spiral agitators during cooling processes, and another was suggested by *Zlokarnik* [47] (Eq. 6) and considers cooling in a common stirring tank. The third one was suggested by *Bel* and *Lallemand* [48] (Eq. 7) and specifically describes the heat transfer for a scrape crystallizer, similarly to the fourth one suggested by *Bott* and *Azoory* [49] (Eq. 8). Liquid properties for water were obtained using calculations provided by the Verein Deutscher Ingenieure (VDI) [50].

$$Nu_{St} = 0.48 * Re_S^{\frac{2}{3}} * Pr^{\frac{1}{3}} * \left(\frac{\eta_{f,m}}{\eta_{W,m}}\right)^{0,14} \quad \text{(Eq. 5)}$$

$$Nu_Z = 0.242 * \left(Re_S * Pr^{\frac{1}{2}} + 4000\right)^{\frac{2}{3}} * \left(\frac{\eta_{f,m}}{\eta_{W,m}}\right)^{0.08} \quad \text{(Eq. 6)}$$

$$Nu_{B\&L} = (Re_a + Re_t)^{0,165} * Pr^{0,211} \quad \text{(Eq. 7)}$$

$$Nu_{B\&A} = C * Re_{fl}^{0.58} * Fr_t^{0.09} * Pr^{0.57} \quad \text{(Eq. 8)}$$

The VDI involves calculating the usual Reynolds number for stirred vessels (Re_S), as listed in Eq. 9 [50]. The axial (Re_a) (Eq. 10) and tangential (Re_t) (Eq.11) Reynolds numbers were, in contrast, used by Bel and Lallemand [48]. Bott and Azoory, in turn, used a flow Reynolds number (Re_f) (Eq. 12) [49]. From the Nusselt correlations, the heat transfer coefficients could be calculated using equation 13.

$$Re_S = \frac{\rho_m * n * {d_{Sc}}^2}{\eta_m} \quad \text{(Eq. 9)}$$

$$Re_a = \frac{\rho_m * u_a * (d_i - d_r)}{\eta_m} \quad \text{(Eq. 10)}$$

$$Re_t = \frac{\rho_m * u_t * d_i}{\eta_m} \quad \text{(Eq. 11)}$$

$$Re_{fl} = \frac{\rho_m * n * d_i * d_e}{\eta_m} \quad \text{(Eq. 12)}$$

$$\alpha = \frac{Nu * \lambda_m}{d_i} \quad \text{(Eq. 13)}$$

Some correlations used different velocities; for example, the axial (u_a) (Eq.14) and the tangential (u_t) (Eq. 15) [48]. Other parameters, such as the equivalent diameter (Eq. 16) and the Froude number (Eq. 17), were used from Bott and Azoory [49].

$$u_a = \frac{4 * q}{\pi * (d_i^2 - d_r^2)} \quad \text{(Eq. 14)}$$

$$u_t = \pi * d_i * n + u_a * \left(\frac{d_{Sc}}{l_{Sc}}\right) \quad \text{(Eq. 15)}$$

$$d_e = 2 * \sqrt{2} * \left(\frac{\dot{m} * \eta_m}{0.0703 * \rho_m^2 * g}\right)^{0.25} \quad \text{(Eq. 16)}$$

$$Fr_t = \frac{n^2 * d_i^2}{d_e * g} \quad \text{(Eq. 17)}$$

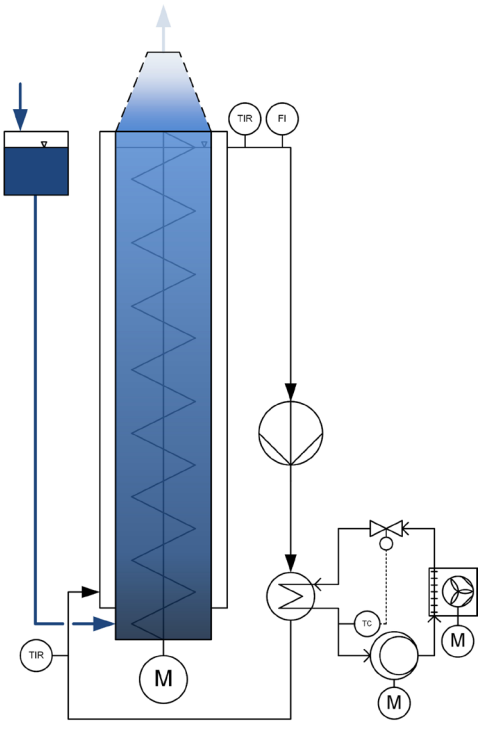

Fig. 5 Schematic flow chart of a screw crystallizer with integrated press section and cooling unit (Color depth indicates the changing concentration)

Because ice particles within the solution can change the overall properties of the suspension, they were considered for all characteristic parameters. For example, the density of the mixture was calculated using an equation from Bel and Lallemand (Eq. 18) [51], where the solid density was calculated using Eq. 19 suggested from *Levy* [52]. The calculation for the heat conductivity of the mixture was suggested by *Brunel* [53] and *Jeffrey* [54] (Eq. 20, Eq. 21, and Eq. 22). Levy [52] published a correlation to calculate the solid heat conductivity for ice water (Eq. 23), as did *Reid* [55] and *Thomas* [56] for the mixture viscosity (Eq. 24).

$$\rho_m = \frac{1}{\frac{w_s}{\rho_s} + \frac{w_l}{\rho_l}} \quad \text{(Eq. 18)}$$

$$\rho_s = 917 * (1 + 1.73 * 10^{-4} * \vartheta) \quad \text{(Eq. 19)}$$

$$\lambda_m = \lambda_l * (1 + 3 * \varphi_s * \beta + 3 * \varphi_s^2 * \beta^2 * \gamma) \quad \text{(Eq. 20)}$$

$$\varepsilon = \frac{\lambda_s}{\lambda_l} \quad \text{(Eq. 21)}$$

$$\gamma = 1 + \left(\frac{\varepsilon - 1}{\varepsilon + 2} * \frac{1}{4}\right) + \left(\frac{3}{16} * \left(\frac{\varepsilon - 1}{\varepsilon + 2}\right) * \left(\frac{\varepsilon + 2}{2 * \varepsilon + 3}\right)\right) \quad \text{(Eq. 22)}$$

$$\lambda_s = 2.24 + 5.975 * 10^{-3} * (-\vartheta)^{1.156} \quad \text{(Eq. 23)}$$

$$\eta_m = \eta_l * \left(1 + 2.5 * \varphi_s + 10.05 * \varphi_s^2 + 0.00273 * e^{(16.6 * \varphi_s)}\right) \quad \text{(Eq. 24)}$$

3.3 Single-step plant (continuous process)

The following single-step plant was designed based on seawater desalination. Since the purification rate to produce potable water from seawater must be around 80, and for well water, between 5 and 10, depending on the source, the design for seawater is more critical, and therefore should be sufficient to produce the process water. Compared to the multi-step plant, a larger plant design with an increased vessel diameter and height, as well as a larger screw, was used. Furthermore, the setup was placed upon a frame designed to absorb and distract the pressing forces. As changeable parameters, the coolant temperature and the screw rotational speed should change the heat transfer, thus increasing the ice mass production and the inner turbulence improving the ice quality. A schematic drawing of the single-step plant can be seen in figure 5.

Table 2 Basic design parameters of the screw crystallizer.

Description	Unit	Parameter
Screw pitch	[°]	47.2
Screw diameter	[m]	0.079
Inner vessel diameter	[m]	0.084
Length cooling area	[m]	0.525
Heat transfer surface	[m²]	0.14
Drive power of gear motor and transmission	[kW]	0.55
Torque of motor and transmission	[Nm]	60
Maximum rotational speed	[1/min]	67
Cooling capacity heat pump	[kWel]	5.5

3.3.1 Experimental setup

The plant consists of several components: a gear motor, different bearings to absorb radial and axial forces, as well as coupling and shaft support to connect the shaft with the drive motor (Fig. 6). The drive motor is equipped with a gear to increase the maximum torque. The connection of the shaft with the shaft support, the coupling, and the attachment of the gear motor is realized via pins.

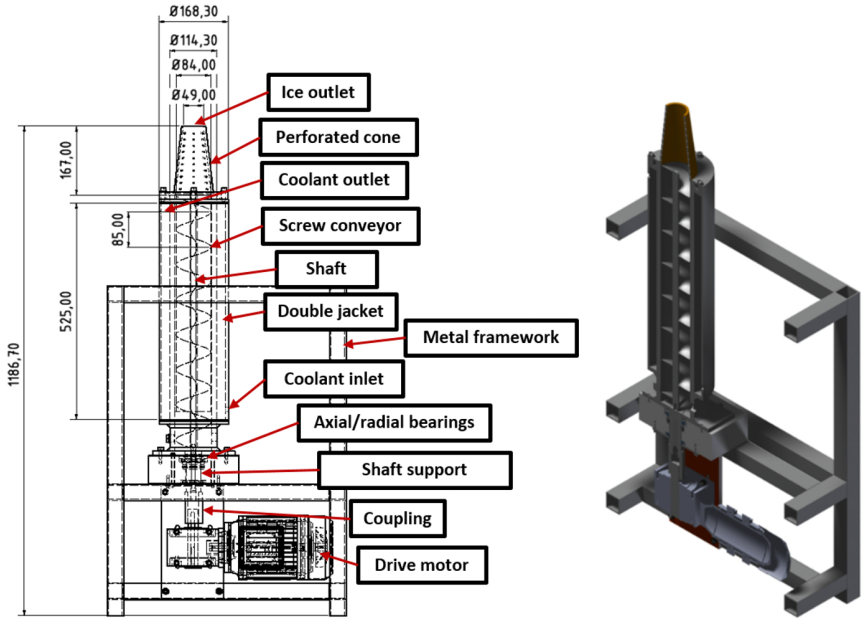

Fig. 6 Technical and sectional drawing of the screw crystallizer with integrated pressing section

The ice, which is produced at the inner surface of the vessel, is transported via the screw conveyor to the upper part of the plant where it is pressed through a perforated, tapering cone. It then leaves the plant as a compact mass, ideally without any inclusions or attached liquid. For cooling purposes, a water/ethylene glycol solution is pumped through the double jacket and cooled down in a separate cooling machine. The coolant then transports along the flow direction of the ice. Therefore, the inlet is installed at the lower and the outlet at the upper part of the vessel.

The dimensions of the crystallizer were chosen by requirements for force absorption (wall thickness, bearings, shaft support, coupling and metal framework) and by available sources (screw, gear motor and heat pump). The parameters of the crystallizer can be seen in table 2.

Table 3 Design parameters for the new screw crystallizer and the perforated, tapered cone

Description	Unit	Parameter			
		Stein	Zlokarnik	Bel & Lallemand	Bott & Azoory
Reynolds number	[-]	Re_S = 550.5		Re_a = 0.15; Re_t = 1848.9	Re_{fl} = 21.1
Nusselt number	[-]	59.7	74.4	5.1	10.6
Inner heat transfer coefficient	[W/(m² K)]	403.3	502.4	34.5	71.5
Heat transition coefficient	[W/(m² K)]	281.7	326.7	33.3	66.4
Heat flow	[W]	760.3	881.8	89.9	179.2
Specific heat flow	[kJ/kg]	411.2			
Outlet diameter of the cone	[m]	≈ 0.084			
Tapering of the cone $\left(\frac{A_o}{A_i}\right)$	[m/m]	≈ 1.00			
Length of the cone	[m]	0.065	0.076	0.008	0.015

Table 4 Final design parameters of the perforated cone

Description	Unit	Parameter
Inlet diameter of the cone	[m]	0.084
Outlet diameter of the cone	[m]	0.049
Tapering of the cone $\left(\frac{A_o}{A_i}\right)$	[m/m]	0.34
Length of the cone	[m]	0.167

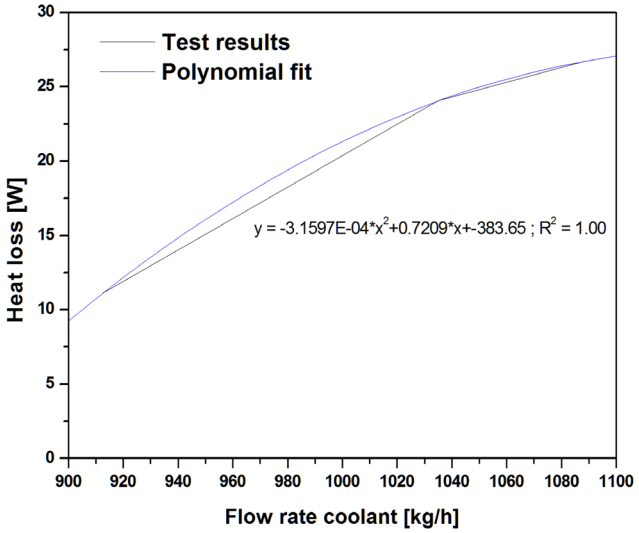

Fig. 7 Heat loss of the crystallizer at a mean coolant temperature of 2 °C for different flow rates

Using the given parameters by the plant, in combination with the Nusselt correlations, the results in plant parameters are shown in table 3. For this, an outer heat transition coefficient of 1,000 W/(m² K) was assumed, as it was achieved during seawater experiments. The coolant inlet temperature was estimated to be around −13.0 °C and the well water around 18.5 °C. This generates a temperature difference of 18.5 K and a logarithmic temperature difference of 19.5 K. Further design parameters, such as the tapering and the length of the cone, can be taken from table 3, which shows that the outer diameter of the cone, as well as the tapering of the cone, has almost no change on the design of the cone. This is due to the low concentration of impurities in the water, causing only a small amount of liquid which is not frozen during the freezing process.

The parameters from Stein and Zlokarnik look reasonable, but the ones from Bel and Lallemand and Bott and Azoory look quite low. Nonetheless, numbers and results from experiments will later be checked for consistency.

The final dimensions of the cone are listed in table 4. Besides the calculated parameters, the cone was designed to desalinate water, which should also be sufficient for well water.

For further calculations, the plant was analyzed for heat losses. This was determined by filling the whole plant with water, then cooled down to 2 °C for different flow rates, then the heat transmission was determined (Fig. 7). Lower temperatures were not possible because of the freezing temperature of water, whereby the amount of frozen water could not have been quantified.

3.3.2 Results and discussion

In section 3.2.1, the described setup is used to investigate different mean coolant temperatures and rotational speeds for their influence on the removal efficiency, heat flow, heat transition coefficient, and crystal area. For this reason, tap water was mixed with several chemicals, as already described in chapter 2. In table 5, all test parameters listed. A rotational speed below 27 1/min was not feasible

Table 5 Test parameters of the screw crystallizer with integrated pressing section

Test	Rotational speed [1/min]	Mean coolant temperature [°C]
1	40	−3.9
2	40	−8.6
3	40	−11.5
4	27	−8.7
5	67	−8.7

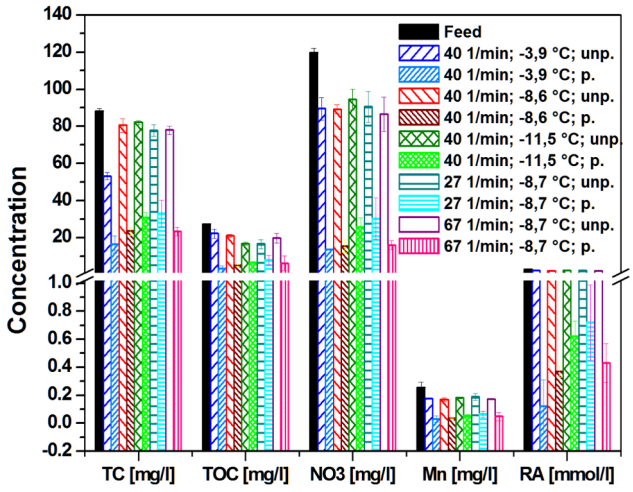

Fig. 8 **Overview of water and ice purity from the feed, the unpressed ice, and the pressed ice for different test parameters**

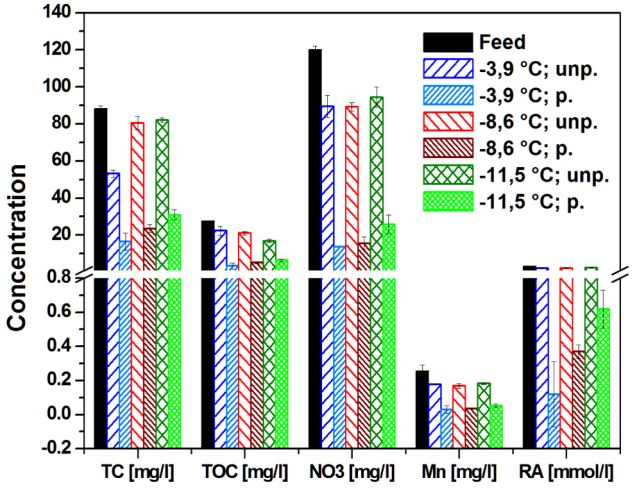

Fig. 9 **Overview of water and ice purity from the feed, the unpressed ice, and the pressed ice for different mean coolant temperatures at a rotational speed of 40 1/min.**

or the gear motor would have been too weak to continually power the screw and pressing the ice. Similar behavior would have been the case for temperatures below −11.5 °C, which is due to the fact that the lower the coolant temperature, the harder the ice gets.

Figure 8 presents an overview of the results for all the test parameters shown. Negative numbers are thereby due to the residual alkalinity, which is calculated as a ratio as shown in equation 4. Obviously, a first purification takes place when the ice is formed and transported upwards. However, most times there is not a significant difference between the feed and the unpressed ice. The largest effect is achieved within the pressing section of the cone, where a significant drop of the concentrations after the ice left the cone can be seen. The best results are achieved when the ice is generated with an average rotational speed and a moderate cooling temperature. All parameters will be discussed in detail.

As can be seen in figure 9, the highest mean coolant temperature gives the best purification results for all impurities. Furthermore, the purification drops with decreasing coolant temperature. Nevertheless, a significant drop of all concentrations below the limit concentration can be seen. Only the total organic carbon concentration is too high, which is due to a very high starting concentration. Unfortunately, the iron concentration could not be measured, due to corrosion.

For an easier perception, all test results for different mean coolant temperatures are also shown in table 6.

As already described, the removal efficiencies are shown as a box plot (Fig. 10). The position of each box varies largely with the mean coolant temperatures, showing that the lower is the temperature, the lower is the removal efficiency. The best value for −3.9 °C is around 96 %, where it is around 88 % and 79 % for −8.6 °C and −11.5 °C, respectively. Furthermore, the spreading of the 25th and 75th percentiles is the least for the highest temperature.

Analysis of the crystallized area also reveals significant differences, depending on the coolant temperature. The deviation of the crystallized areas of the unpressed ice is rather small compared to the ones from the pressed ice, where the differences are quite clear. Furthermore, the higher the crystal area is the better the quality is of the ice. This indicates that any inclusions or attached liquid is pressed away by the volume reduction within the cone. It also shows that the crystal area is a characteristic for the purification rate.

Observation of the heat flow shows that, with increasing coolant temperatures, the heat flow decreases, as expected. Also, an expected behavior shows the heat transition coefficient, which drops when the heat flow increases. This is due to a higher amount of produced ice mass within the vessel, and thus a lower turbulence. Overall, it shows that changing the coolant temperature influences the heat, and thus the product flow, as well as the purity, due to

Table 6 **Overview of the test results from experiments with different mean coolant temperatures at a rotational speed of 40 1/min**

Parameters	Unit	Feed	−3.9 °C		−8.6 °C		−11.5 °C	
			unpressed	pressed	unpressed	pressed	unpressed	pressed
TC	[mg/l]	88.2	53.2	16.4	80.5	23.5	82.1	30.9
TOC	[mg/l]	27.6	22.3	3.29	21.0	5.10	16.8	6.40
NO3	[mg/l]	120.0	89.5	13.7	89.2	15.5	94.5	25.7
Mn	[mg/l]	0.255	0.176	0.03	0.169	0.034	0.182	0.053
RA	[°dH]	16.9	12.2	0.66	12.0	2.10	12.8	3.50

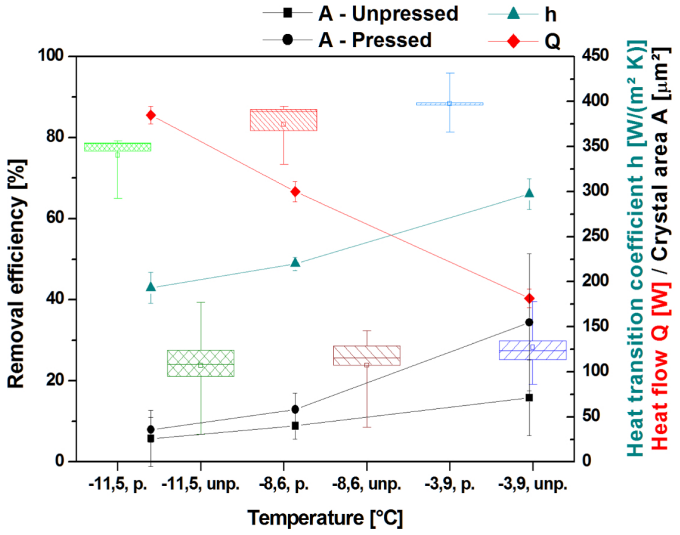

Fig. 10 Removal efficiency, heat transmission coefficient, heat flow, and crystal area for different mean coolant temperatures at a screw rotational speed of 40 1/min

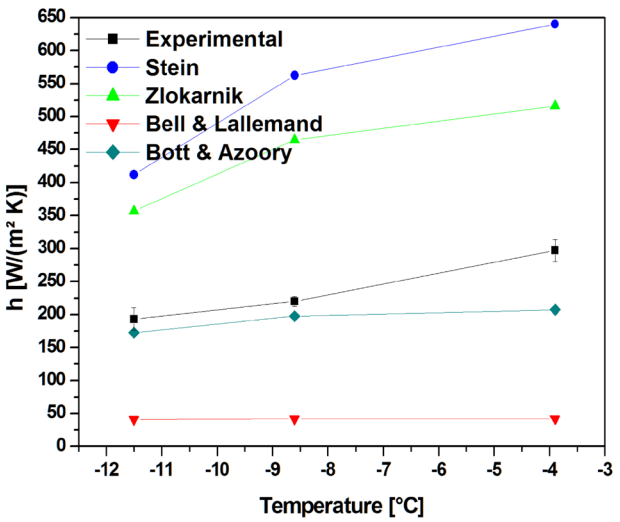

Fig. 11 Overview of heat transition coefficients determined experimentally and calculated depending on the mean coolant temperature, at a screw rotational speed of 40 1/min

turbulences preventing the formation of a concentration gradient next to the ice front.

Also interestingly, no liquid inclusions in the images of ice particles are visible. Only liquid surrounding the crystal and its ramifications can be observed, which might be due to the small size of the crystal, a result of the scraping. The larger side of the crystal was formed during scratching and the thin side during crystal growth (Fig. 2).

Based on the measured outer heat transfer coefficient, the heat transition coefficient for each Nusselt correlation was calculated and compared to the experimental value (Fig. 11). No correlations from Stein, Zlokarnik, or Bel and Lallemand fit with the experimental values. The correlation from Bott and Azoory, conversely, fit quite well. Only the correlation for the lowest coolant temperature is significantly different from the calculated one. The differences may have been caused by a missing value in the calculations, considering the ice fraction and the accumulation of the ice, which is not known exactly but occurs because of the pressing resistance caused by the cone.

Varying the rotational speed of the screw should change the turbulence within the vessel, and, therefore, the flow caused by a larger heat transition coefficient. This, in turn, should improve the ice purity because of a lower concentration gradient next to the growing ice front. All results can be seen in figure 12 and table 7.

The concentration of the unpressed ice is, again, slightly lower than the feed; however, most of the purification takes place within the cone. Nevertheless, increasing the rotational speed improves the purification in the first step, but further increase does not further enhance the results.

The cause for this behavior can be seen in figure 13. The heat flow, as well as the heat transition coefficient, increase when the rotational speed is raised from 27 1/min to 40 1/min. This can be expected due to an increased turbulence of the liquid. It also shows an increase in the ice crystal area, indicating a better removal efficiency. A further increase to 67 1/min does not improve the heat flow, transition coefficient, or the crystal area, and thus, the removal efficiency. Apparently, a higher rotational speed leads to a collapse in the turbulence and the corresponding consequences for all other factors. This cannot be due to the ice mass because of the lower heat flow, which is even lower than for 27 1/min. It is more likely that the radial upwards flow, caused by the screw, gets disturbed by flow separation and/or the higher axial flow. Unfortunately, the reason cannot be determined in detail with this plant.

A comparison of experimental and calculated heat transition coefficients show a similar curve characteristic as the previous coefficients (Fig. 14). The results from Stein and Zlokarnik appear too high, whereas the one from Bel and Lallemand is too low, and

Table 7 Overview of the test results from experiments with different rotational speeds at mean coolant temperature of –8.7 °C

Parameters	Unit	Feed	27 1/min		40 1/min		67 1/min	
			unpressed	pressed	unpressed	pressed	unpressed	pressed
TC	[mg/l]	88.2	77.7	33.0	80.5	23.5	77.9	23.4
TOC	[mg/l]	27.6	16.6	7.90	21.0	5.10	19.8	6.20
NO_3	[mg/l]	120.0	90.5	30.4	89.2	15.5	86.5	16.0
Mn	[mg/l]	0.255	0.188	0.064	0.169	0.034	0.172	0.048
RA	[°dH]	16.9	12.5	4.00	12.0	2.10	11.8	2.40

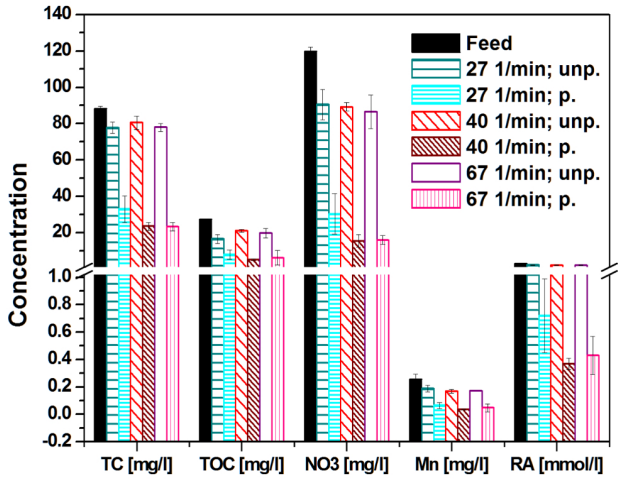

Fig. 12 Overview of water and ice purity from the feed, the unpressed ice and pressed ice for different rotational speeds at a mean coolant temperature of –8.7 °C

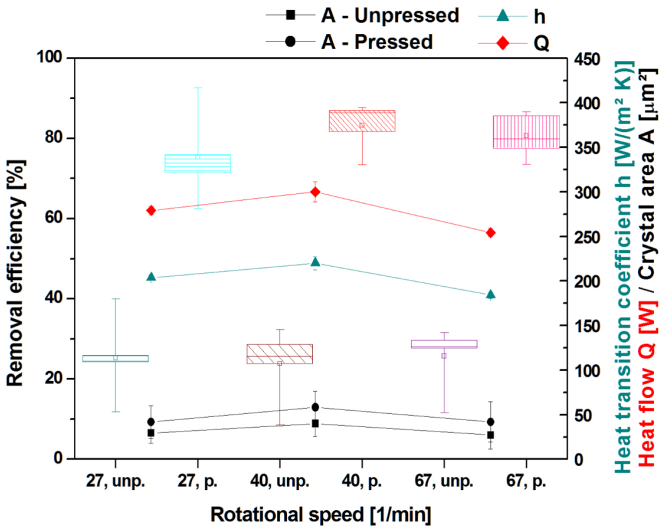

Fig. 13 Removal efficiency, heat transmission coefficient, heat flow and crystal area for different rotational speeds at a mean coolant temperature of –8.7 °C

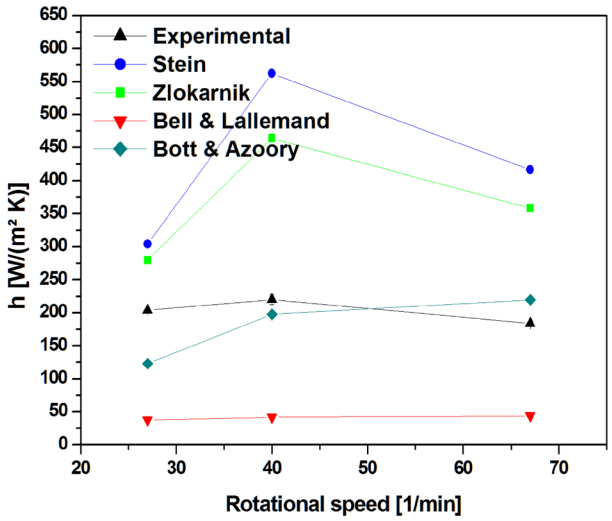

Fig. 14 Overview of heat transition coefficients determined experimentally and calculated based on the rotational speed at a mean coolant temperature of –8.7 °C

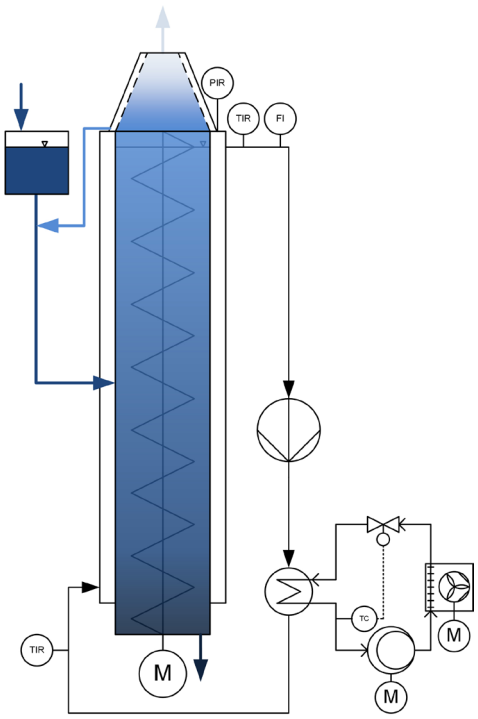

Fig. 15 Schematic flow chart of an optimized screw crystallizer with integrated press section and cooling unit (Color depth indicates the changing salt concentration)

does not really change with increasing rotational speed. Again, the correlation from Bott and Azoory shows the best accordance.

For further plant designs, the correlation from Bott and Azoory appear within reasonable limits. This is underpinned by the fact that the mean outer heat transfer coefficient was around 1,254.3 W/(m² K), which is slightly better than estimated, but still indicates that the limiting factor is the inner heat transfer.

3.4. Test plant optimizations

Further optimizations on the test plant will help investigate heat transfer, depending on various parameters, and help improve purification with even higher mass flow rates (Fig. 15). Therefore, a new screw will be designed that will have a smaller gap between vessel and screw, to faster convey the ice upwards. An installed return of the press water and a purge will prevent accumulation of impurities within the liquid and will guarantee a continuous process. Furthermore, a sensor for force measurement will show the dependencies of parameter variations, the corresponding force, and thus, the influence on the ice quality.

4 Conclusions

Investigation of a new method for water purification by utilizing well water to produce process water for the brewing industry shows good results with regards to removal efficiency. It even allows for

adjusting the process parameters, depending on the water source and the necessary purification rate. Further, in contrast to other freeze crystallization plants, this new method prevents the loss of product through washing the ice.

The multi-step process in this method, consisting of a commercial scraped surface crystallizer in combination with a cooled pressing mold, showed that the application of a force of 7.7 kN (20.6 bar) for a holding time of 300 s was sufficient for purification.

Another investigation, based on a seawater desalination plant, was designed, with a screw as a forced conveyor, and a perforated, tapering cone for pressing, to determine if water purification can be achieved by a single-step process. Experiments showed good results depending on ice purities, heat flows, heat transition coefficients, and crystal sizes from rotational speeds and coolant temperatures. Comparing these results with correlations from the literature showed that the correlation from Bott and Azoory could be used to design a single-step plant.

Further optimizations of the plant including a purge, a return flow, a force measurement, and an improved screw design will help find design parameters for such plants. It will also allow more tests to determine whether this kind of method can also be used to purify waste water from the brewing industry, with its high loads.

However, this plant was built to investigate whether the technology can be used to purify water for a possible use in the brewing process. Related to this, these tests will help to develop and commercialize a plant as an alternative product to reverse osmosis and ion exchanger technologies.

Acknowledgments

This work was funded by the German Federal Ministry for Economic Affairs and Energy (AiF Project GmbH, Funding Code KF 2035726 SA3).

5 References

1. Townsend, G.: Building a Water Resilient Future, BRAUWELT International, **36** (2018), no. 1, pp. 22-24.
2. Casani, S.; Rouhany, M. and Knøchel, S.: A discussion paper on challenges and limitations to water reuse and hygiene in the food industry, Water Research, **39** (2005), no. 6, pp. 1134-1146.
3. Pettigrew, L.; Blomenhofer, V.; Hubert, S.; Groß, F. and Delgado, A.: Optimisation of water usage in a brewery clean-in-place system using reference nets, Journal of Cleaner Production, **87** (2015), no. 1, pp. 583-593.
4. Fillaudeau, L.; Blanpain-Avet, P. and Daufin, G.: Water, wastewater and waste management in brewing industries, Journal of Cleaner Production, **14** (2006), no. 5, pp. 463-471.
5. Brewers Association: Water and Wastewater: Treatment/Volume Reduction Manual 2017.
6. Donoghue, C.; Jackson, G.; Koop, J.H. and Heuven, A.J.M.: The Environmental Performance of the European Brewing Sector 2012.
7. Sturm, B.; Hugenschmidt, S.; Joyce, S.; Hofacker, W. and Roskilly, A.P.: Opportunities and barriers for efficient energy use in a medium-sized brewery, Applied Thermal Engineering, **53** (2013), no. 2, pp. 397-404.
8. Narziss, L. and Back, W.: Brauwissenschaft und Brauereitechnologie, Chemie-Ingenieur-Technik, **88** (2016), no. 12, pp. 1869-1879.
9. Zufall, C. and Tyrell, T.: The Influence of Heavy Metal Ions on Beer Flavour Stability, Journal of Institute of Brewing, **114** (2008), no. 2, pp. 134-142.
10. Cerrato, J.M.; Falkinham, J.O.; Dietrich, A.M.; Knocke, W.R.; McKinney, C.W. and Pruden, A.: Manganese-oxidizing and -reducing microorganisms isolated from biofilms in chlorinated drinking water systems, Water Research, **44** (2010), no. 13, pp. 3935-3945.
11. Bhatnagar, A. and Sillanpää, M.: A review of emerging adsorbents for nitrate removal from water, Chemical Engineering Journal, **168** (2011), no. 2, pp. 493-504.
12. Tankiewicz, M. and Biziuk, M.: Fast , sensitive and reliable multi-residue method for routine determination of 34 pesticides from various chemical groups in water samples by using dispersive liquid – liquid microextraction coupled with gas chromatography – mass spectrometry, **410** (2018), no. 5, pp. 1533-1550.
13. Franke, M. and Birmelin, M.: Brauwasseraufbereitung mit Umkehrosmose (Teil 2), BRAUWELT, **153** (2013), no. 23, pp. 672-674.
14. Cipollina, A.; Micale, G. and Rizzuti, L.: Seawater Desalination for Freshwater Production, Seawater Desalination, 2009.
15. Erlbeck, L.; Rädle, M.; Nessel, R.; Illner, F.; Müller, W.; Rudolph, K.; Kunz, T. and Methner, F.-J.: Investigation of the depletion of ions through freeze desalination, Desalination, **407** (2017), pp. 93-102.
16. Anand, S.; Gupta, A. and Tyagi, S.K.: Solar cooling systems for climate change mitigation: A review, Renewable and Sustainable Energy Reviews, **41** (2015), pp. 143-161.
17. Karagiannis, I.C. and Soldatos, P.G.: Water desalination cost literature: review and assessment, Desalination, **223** (2008), no. 1-3, pp. 448-456.
18. Marrero, G. a. and Ramos-Real, F.J.: Electricity generation cost in isolated system: The complementarities of natural gas and renewables in the Canary Islands, Renewable and Sustainable Energy Reviews, **14** (2010), no. 9, pp. 2808-2818.
19. Erlbeck, L.; Nessel, R.; Illner, F.; Müller, W.; Kunz, T.; Schuchmann, H.; Rädle, M. and Methner, F.-J.: Commercial feasibility of a new freeze crystallization plant for small-scale potable water production, Desalination and Water Treatment, **105** (2018), pp. 23-34.
20. Younos, T. and Tulou, K.: Overview of desalination techniques, Journal of Contemporary Water Research & Education, **132** (2005), no. 1, pp. 3-10.
21. Steinbach, A.: Gewinnung von Trinkwasser aus Meerwasser durch Ausfrieren, Chemie Ingenieur Technik, (1951), pp. 296-298.
22. Breitner, H.J.: Entmischung beim Gefrieren wässeriger Lösungen, Deutsche Hydrografische Zeitschrift, (1953).
23. Halde, R.: Concentration of impurities by progressive freezing, Water Research, **14** (1980), no. 6, pp. 575-580.
24. Khajehei, F.; Niakousari, M.; Eskandari, M.H. and Sarshar, M.: Production of Pomegranate Juice Concentrate by Complete Block Cryoconcentration Process, Journal of Food Process Engineering, **38** (2015), no. 5, pp. 488-498.
25. Orellana-Palma, P.; Petzold, G.; Andana, I.; Torres, N. and Cuevas, C.: Retention of ascorbic acid and solid concentration via centrifugal freeze concentration of orange juice, Journal of Food Quality, (2017).
26. Orellana-Palma, P.; Petzold, G.; Guerra-Valle, M. and Astudillo-Lagos, M.: Impact of block cryoconcentration on polyphenol retention in blueberry juice, Food Bioscience, **20** (2017), pp. 149-158.
27. Hartel, R.W. and Espinel, L.A.: Freeze concentration of skim milk, Journal of Food Engineering, **20** (1993), no. 2, pp. 101-120.

28. Sánchez, J.; Hernández, E.; Auleda, J.M. and Raventós, M.: Freeze concentration of whey in a falling-film based pilot plant: Process and characterization, Journal of Food Engineering, **103** (2011), no. 2, pp. 147-155.
29. Moreno, F.L.; Raventós, M.; Hernández, E. and Ruiz, Y.: Behaviour of falling-film freeze concentration of coffee extract, Journal of Food Engineering, **141** (2014), pp. 20-26.
30. Moreno, F.L.; Hernández, E.; Raventós, M.; Robles, C. and Ruiz, Y.: A process to concentrate coffee extract by the integration of falling film and block freeze-concentration, Journal of Food Engineering, **128** (2014), pp. 88-95.
31. Moreno, F.L.; Raventós, M.; Hernández, E. and Ruiz, Y.: Block freeze-concentration of coffee extract: Effect of freezing and thawing stages on solute recovery and bioactive compounds, Journal of Food Engineering, **120** (2014), no. 1, pp. 158-166.
32. Moreno, F.L.; Quintanilla-Carvajal, M.X.; Sotelo, L.I.; Osorio, C.; Raventós, M.; Hernández, E. and Ruiz, Y.: Volatile compounds, sensory quality and ice morphology in falling-film and block freeze concentration of coffee extract, Journal of Food Engineering, **166** (2015), pp. 64-71.
33. Robles, C.M.; Quintanilla-Carvajal, M.X.; Moreno, F.L.; Hernández, E.; Raventós, M. and Ruiz, Y.: Ice morphology modification and solute recovery improvement by heating and annealing during block freeze-concentration of coffee extracts, Journal of Food Engineering, **189** (2016), pp. 72-81.
34. Pazmiño, N.; Raventos, M.; Hernández, E.; Gulfo, R.; Robles, C.; Moreno, F.L. and Ruiz, Y.: Continuous system of freeze concentration of sucrose solutions: Process parameters and energy consumption., Journal of Food Technology and Preservation, **1** (2016), no. 1, pp. 1-5.
35. Shirai, Y.; Wakisakay, M.; Miyawak, O. and Sakashita, S.: Conditions of Producing an Ice Layer with High Purity for Freeze Wastewater Treatment, Journal of Food Engineering, **38** (1999), no. 1998, pp. 297-308.
36. Shirai, Y.; Wakisaka, M.; Miyawaki, O. and Sakashita, S.: Effect of seed ice on formation of tube ice with high purity for a freeze wastewater treatment system with a bubble-flow circulator, **33** (1999), no. 5, pp. 1325-1329.
37. Hirata, T.; Matsuzaki, Y. and Ishikawa, M.: Ice formation of aqueous solution and its removal phenomena on vertical cooled plate, Heat and Mass Transfer, **40** (2003), no. 11, pp. 829-834.
38. Okawa, S.; Ito, T. and Saito, A.: Effect of crystal orientation on freeze concentration of solutions, International Journal of Refrigeration, **32** (2009), no. 2, pp. 246-252.
39. Gao, W. and Shao, Y.: Freeze concentration for removal of pharmaceutically active compounds in water, Desalination, **249** (2009), no. 1, pp. 398-402.
40. Avramidis, P.; Nikolaou, K. and Bekiari, V.: Total Organic Carbon and Total Nitrogen in Sediments and Soils: A Comparison of the Wet Oxidation – Titration Method with the Combustion-infrared Method, Agriculture and Agricultural Science Procedia, **4** (2015), pp. 425-430.
41. Xie, Z.; He, J.; Lü, C.; Zhang, R.; Zhou, B.; Mao, H.; Song, W.; Zhao, W.; Hou, D.; Wang, J. and Li, Y.: Organic carbon fractions and estimation of organic carbon storage in the lake sediments in Inner Mongolia Plateau, China, Environmental Earth Sciences, **73** (2015), no. 5, pp. 2169-2178.
42. Gupta, S.K.; Gupta, R.C.; Gupta, a B.; Seth, a K.; Bassin, J.K. and Gupta, A.: Recurrent acute respiratory tract infections in areas with high nitrate concentrations in drinking water., Environmental Health Perspectives, **108** (2000), no. 4, pp. 363-366.
43. National Institute of Health: ImageJ2017.
44. Franke, M. and Birmelin, M.: Brauwasser: Beschaffenheit und Aufbereitung (Teil 1), BRAUWELT, **153** (2013), no. 18-19, pp. 535-537.
45. Stamatiou, E.; Meewisse, J.W. and Kawaji, M.: Ice slurry generation involving moving parts, International Journal of Refrigeration, **28** (2005), no. 1, pp. 60-72.
46. Stein, W.A.: Rührleistung und Wärmeübergang auf der Innenseite eines Rührbehälters mit verschiedenen Wendel-Rührern, Engineering Research, **59** (1993), no. 9, pp. 165-172.
47. Zlokarnik, M.: Wärmeübergang an der Wand eines Rührbehälters beim Kühlen und Heizen im Bereich $10^0 < Re < 10^5$, Chemie Ingenieur Technik, **22** (1969), pp. 1195-1242.
48. Bel, O. and Lallemand, A.: Etude d'un fluide frigoporteur diphasique 2: Analyse expérimentale du comportement thermique et rhéologique, International Journal of Refrigeration, **22** (1999), pp. 175-187.
49. Bott, T.R. and Azoory, S.: Heat transfer in scraped heat exchangers, Chemical and Process Engineering, (1969), pp. 85-87.
50. VDI-Gesellschaft Verfahrenstechnik und Chemieingenieurwesen: VDI-Wärmeatlas, 2010.
51. Bel, O. and Lallemand, A.: Etude d'un fluide frigoporteur diphasique 1: Caractéristiques thermophysiques intrinsèques d'un coulis de glace, International Journal of Refrigeration, **22** (1999), pp. 164-174.
52. Levy, F.L.: Calculating the thermal conductivity of meat and fish in the freezing range, International Journal of Refrigeration, **5** (1982), no. 3, pp. 149-154.
53. Brunel, R.F. and Van Bibber, K.: Density and thermal expansion of liquid organic compounds under atmospheric pressure, International Critical Tables of Numerical Data Physics, Chemistry and Technology, 1933, p. 27.
54. Jeffrey, D.J.: Conduction Through a Random Suspension of Spheres, Proceedings of the Royal Society A: Mathematical, Physical and Engineering Sciences, **335** (1973), no. 1602, pp. 355-367.
55. Reid, R.C.; Prausnitz, J.M. and Poling, B.E.: The properties of gas and liquids, 1986.
56. Thomas, D.G., 1965.: Transport characteristics of suspension: VIII. A note on the viscosity of Newtonian suspensions of uniform spherical particles, Journal of Colloid Science, **20** (1969), no. 3, pp. 267-277.

Received 30 June 2018, accepted 7 August 2018